



doi:10.1016/S0016-7037(03)00105-4

Reaction-based modeling of quinone-mediated bacterial iron(III) reduction

WILLIAM D. BURGOS,^{1,*} YILIN FANG,¹ RICHARD A. ROYER,¹ GOUR-TSYH YEH,² JAMES J. STONE,¹ BYONG-HUN JEON,¹ and BRIAN A. DEMPSEY¹¹Department of Civil and Environmental Engineering, Pennsylvania State University, 212 Sackett Building, University Park, PA 16802-1408, USA²Department of Civil and Environmental Engineering, University of Central Florida, 4000 Central Florida Blvd., Orlando, FL 32816-2450, USA

(Received August 19, 2002; accepted in revised form January 10, 2003)

Abstract—This paper presents and validates a new paradigm for modeling complex biogeochemical systems using a diagonalized reaction-based approach. The bioreduction kinetics of hematite (α -Fe₂O₃) by the dissimilatory metal-reducing bacterium (DMRB) *Shewanella putrefaciens* strain CN32 in the presence of the soluble electron shuttling compound anthraquinone-2,6-disulfonate (AQDS) is used for presentation/validation purposes. Experiments were conducted under nongrowth conditions with H₂ as the electron donor. In the presence of AQDS, both direct biological reduction and indirect chemical reduction of hematite by bioreduced anthrahydroquinone-2,6-disulfonate (AH₂DS) can produce Fe(II). Separate experiments were performed to describe the bioreduction of hematite, bioreduction of AQDS, chemical reduction of hematite by AH₂DS, Fe(II) sorption to hematite, and Fe(II) biosorption to DMRB. The independently determined rate parameters and equilibrium constants were then used to simulate the parallel kinetic reactions of Fe(II) production in the hematite-with-AQDS experiments. Previously determined rate formulations/parameters for the bioreduction of hematite and Fe(II) sorption to hematite were systematically tested by conducting experiments with different initial conditions. As a result, the rate formulation/parameter for hematite bioreduction was not modified, but the rate parameters for Fe(II) sorption to hematite were modified slightly. The hematite bioreduction rate formulation was first-order with respect to hematite "free" surface sites and zero-order with respect to DMRB based on experiments conducted with variable concentrations of hematite and DMRB. The AQDS bioreduction rate formulation was first-order with respect to AQDS and first-order with respect to DMRB based on experiments conducted with variable concentrations of AQDS and DMRB. The chemical reduction of hematite by AH₂DS was fast and considered to be an equilibrium reaction. The simulations of hematite-with-AQDS experiments were very sensitive to the equilibrium constant for the hematite-AH₂DS reaction. The model simulated the hematite-with-AQDS experiments well if it was assumed that the ferric oxide "surface" phase was more disordered than pure hematite. This is the first reported study where a diagonalized reaction-based model was used to simulate parallel kinetic reactions based on rate formulations/parameters independently obtained from segregated experiments. Copyright © 2003 Elsevier Ltd

1. INTRODUCTION

Combined biologic-chemical reactions are a common feature of biogeochemical systems. For example, dissimilatory metal-reducing bacteria (DMRB) can biologically reduce and dissolve ferric oxides and the biogenic Fe(II) can then chemically react with other reducible compounds in the system. Reducible compounds of concern include organic contaminants such as chlorinated aliphatics (Kim and Picardal, 1999) and nitroaromatics (Klausen et al., 1995), and inorganic contaminants such as arsenate (Cummins et al., 1999; Langner and Inskeep, 2000), chromate (Fendorf and Li, 1996), Co(III) (Caccavo et al., 1994; Brooks et al., 1999), Tc(VII) (Wildung et al., 2000) and U(VI) (Lovley et al., 1991; Fredrickson et al., 2000). With most of these inorganic contaminants, the DMRB can also use the oxidized metal/radionuclide as an electron acceptor. Thus, both "direct" (biologic) and "indirect" (combined biologic-chemical) mechanisms can lead to inorganic contaminant reduction.

The relative importance of either the direct or indirect reduction mechanism on contaminant fate under iron-reducing

conditions is difficult to resolve. From a mathematical modeling perspective, parallel kinetic reactions that produce the same product [e.g., Fe(II) from Fe(III) via DMRB activity or via reaction with bioreduced quinones] cannot be uniquely segregated (Yeh et al., 2001). Individual rate formulations cannot be established for either parallel process unless experimental systems are designed such that only one of the kinetic reactions is operative at a time. Another complicating factor in iron-reducing environments is that the reactivity of the contaminant will be strongly linked to the reducing power of the biogenic Fe(II) species. Biogenic Fe(II) could exist as Fe²⁺(aq), soluble Fe(II) complexes, mineral-sorbed Fe(II), biosorbed Fe(II) or as an Fe(II)-containing mineral. The reducing power and contaminant specificity will likely vary with each Fe(II) species (Liger et al., 1999), thus a whole suite of parallel kinetic reactions leading to contaminant reduction may be operative.

One approach to studying biogeochemical systems that contain parallel kinetic reactions is to experimentally isolate each process and determine reaction-based rate formulations/parameters for each kinetic reaction in what we term "segregated" experiments. After reaction-based rate formulations/parameters are determined from simpler segregated experiments, the more complicated "combined" kinetics experiment would be performed (i.e., system has the multiple reactions from the segre-

* Author to whom correspondence should be addressed (wdb3@psu.edu).

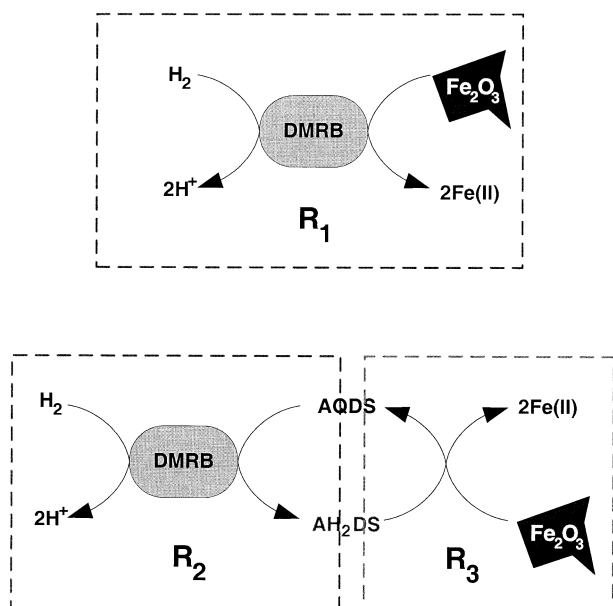


Fig. 1. Bioreduction of hematite (α - Fe_2O_3) by dissimilatory iron-reducing bacteria (DMRB) in the presence of anthraquinone-2,6-disulfonate (AQDS). Parallel kinetic reactions both lead to the production of Fe(II). Separate experiments were conducted to uniquely evaluate each reaction (represented by dashed boxes). Reaction numbers correspond to reaction network proposed in Table 1.

gated experiments occurring in parallel). The combined kinetics experiment would not be used for any rate parameterization purposes. Instead, all independently determined reaction-based rate formulations/parameters would be included in a mathematical model to simulate the combined kinetics experiment. A successful simulation would serve to validate the individual rate formulations/parameters and the overall theoretical approach.

The focus of this paper is to present and validate a new paradigm for modeling complex biogeochemical systems. The bioreduction kinetics of hematite (α - Fe_2O_3) by *Shewanella putrefaciens* strain CN32 in the presence of the soluble electron shuttling compound anthraquinone-2,6-disulfonate (AQDS) will be used for presentation/validation purposes. The addition of soluble electron shuttling compounds are known to stimulate the rate and extent of reduction of both crystalline (Zachara et al., 1998; Royer et al., 2002) and non-crystalline iron oxides (Lovley et al., 1996; Fredrickson et al., 1998). When both hematite and AQDS are included in an experiment two parallel kinetic reactions produce Fe(II); direct biologic reduction and indirect chemical reduction by bioreduced anthrahydroquinone-2,6-disulfonate (AH_2DS ; R1 and R2+R3, respectively, in Fig. 1 and Table 1) because, as noted by inspection of Eqn. 2.1 in Table 1, the relative contributions of these two reactions could not be segregated. Therefore, separate experiments were designed and performed to individually parameterize these reactions. In a recent related study (Burgos et al., 2002), reaction-based kinetic rate formulations for R1 and the sorption of Fe(II) to hematite (R7 + R8 + R9), and an equilibrium constant for the biosorption of Fe(II) to *S. putrefaciens* CN32 (R10) were determined. While there are many possible mechanisms for biologic iron reduction [e.g., direct contact between

membrane-bound proteins and the oxide surface, soluble extracellular electron shuttles, and/or solubilization and intracellular transport of Fe(III)], for our purposes R1 represents the net activity of these biologic pathways. In the current study, additional experiments were used to systematically test, validate and, for one reaction, refine the previously determined rate parameters (rate formulations were unchanged), and to develop reaction-based formulations for the additional reactions R2 and R3. All these independently determined rate formulations/parameters were then included in the reaction-based biogeochemical model BIOGEOCHEM (Fang et al., 2003) and used to predict, without reformulation or recalibration, the combined kinetics experiment (i.e., hematite-with-AQDS).

2. MODELING METHODS

The reaction network for equilibrium reactions written in matrix forms dates back to the late 1970s—early 1980s (e.g., Smith, 1980). When mass conserved components are chosen a priori and the reaction network is relatively simple, the network can easily be written in canonical form manually. However, when the reaction network becomes more complex such a reduction is not manually straightforward, and a systematic reduction to canonical form is required. Smith (1980) discussed the efficient calculation of a reaction stoichiometry matrix (defined below in Eqn. 16) in the canonical form when all reactions are fast and linearly independent. When the reactions involve both equilibrium and kinetic reactions and many parallel reactions are present in the system, the means to achieve the reduction were first discussed in the early 1990s (e.g., Chen, 1994; Chilakapati, 1995).

Reaction-based models formulate the production-consumption rate of every chemical species due to every chemical reaction (both equilibrium and kinetic) for a specified reaction network. The reaction network contains M chemical species (out of the M species, N_C species are considered component species) that are defined by N_E independent equilibrium reactions, N_K independent kinetic reactions, and N_C independent components. The formal selection of N_C chemical components and the determination of N_I linearly-independent reactions ($N_I = M - N_C$) are made by an automated reaction matrix diagonalization-decomposition procedure using the Gauss-Jordan elimination (Steeffel and Macquarrie, 1996; Chilakapati et al., 1998) as part of the BIOGEOCHEM preprocessor (Fang et al., 2003). The matrix decomposition formally decouples equilibrium (i.e., “fast”) reactions from kinetic (i.e., “slow”) reactions, enforces mass conservation of chemical components, and segregates the kinetic reactions.

Most importantly, when parallel kinetic reactions are not present, the matrix diagonalization-decomposition segregates all kinetic reactions such that rate formulations/parameters are determined one reaction at a time, completely independent of all other kinetic reactions. The individual rate formulation and parameter estimation/optimization for each and every kinetic reaction is possible only when reaction-based modeling is coupled with the diagonalization-decomposition procedure. An advantage of using such an approach then is that the rate formulations/parameters are theoretically descriptive of the chemical reaction and, therefore, applicable to a range of environmental conditions (versus only those of the experiment).

Table 1. Reaction network, matrix decomposition and reaction-based rate formulations for the bioreduction of hematite-with-AQDS. All Fe species are in (+III) valence unless designated Fe^(II) or Fe²⁺.

Reaction	Reaction Number	Reaction Parameters
Bacterial Reduction of Hematite Fe ₂ O ₃ + H ₂ (aq) + 4H ⁺ ⇌ 2Fe ²⁺ + 3H ₂ O	(R1)	Eq. 4.1
Bacterial Reduction of AQDS AQDS + H ₂ (aq) ⇌ AH ₂ DS	(R2)	Eq. 4.2a
Chemical Reduction of Hematite by AH ₂ DS AH ₂ DS + Fe ₂ O ₃ + 4H ⁺ ⇌ AQDS + 2Fe ²⁺ + 3H ₂ O	(R3)	logK ₃ ^e = +18.03
Surface "Hydration" of Hematite Fe ₂ O ₃ + 3H ₂ O ⇌ 2[(OH) ₂ =FeOH]	(R4)	logK _{TSS} ^e = -1.91
Hematite Surface Acidity =FeOH ₂ ⁺ ⇌ =FeOH + H ⁺	(R5)	logK ₅ ^e = -7.31
=FeOH ⇌ =FeO + H ⁺	(R6)	logK ₆ ^e = -8.93
Sorption of Fe ²⁺ to Hematite =FeOH ₂ ⁺ + Fe ²⁺ ⇌ =FeOFe ^{(II)+} + 2H ⁺	(R7)	R7+R8+R9 → Eq. 4.3
=FeOH + Fe ²⁺ ⇌ =FeOFe ^{(II)+} + H ⁺	(R8)	
FeO + Fe ²⁺ ⇌ =FeOFe ^{(II)+}	(R9)	
Biosorption of Fe ²⁺ DMRB + Fe ²⁺ ⇌ DMRB-Fe ²⁺	(R10)	logK ₁₀ ^e = +1.43
PIPES Buffering HPIPES ⇌ PIPES + H ⁺	(R11)	logK ₁₁ ^e = -6.80
N _E Mass Action Equations		
	$K_3^e = \frac{[\text{AQDS}][\text{Fe}^{2+}]^2}{[\text{H}^+]^4[\text{AH}_2\text{DS}]}$	(1.1)
	$K_4^e = \frac{[=\text{FeOH}]_T}{[\text{Fe}_2\text{O}_3]}$	(1.2) ^A
	$K_5^e = \frac{[=\text{FeOH}][\text{H}^+]}{[=\text{FeOH}_2^+]}$	(1.3)
	$K_6^e = \frac{[=\text{FeO}^-][\text{H}^+]}{[=\text{FeOH}]}$	(1.4)
	$K_{10}^e = \frac{[\text{DMRB}-\text{Fe}^{2+}]}{[\text{DMRB}][\text{Fe}^{2+}]}$	(1.5)
	$K_{11}^e = \frac{[\text{PIPES}^-][\text{H}^+]}{[\text{HPIPES}]}$	(1.6)
N _K Kinetic-Variable Equations		
	$\frac{1}{2} \frac{d([\text{Fe}^{2+}] + [=\text{FeOFe}^{(II)+}] + [\text{DMRB}-\text{Fe}^{2+}] + 2[\text{AH}_2\text{DS}])}{dt} = R_1 + R_2$	(2.1)
	$\frac{d[=\text{FeOFe}^{(II)+}]}{dt} = R_7 + R_8 + R_9$	(2.2)
N _C Mass Conservation Equations		
	$\text{TOT}_{\text{Fe}_{203}} = \frac{1}{2}([=\text{FeOH}_2^+] + [=\text{FeOH}] + [=\text{FeO}^-] + [\text{Fe}^{2+}] + [\text{DMRB}-\text{Fe}^{2+}] + [\text{Fe}_2\text{O}_3] + [=\text{FeOFe}^{(II)+}])$	(3.1)
	$\text{TOT}_{\text{AQDS}} = [\text{AQDS}] + [\text{AH}_2\text{DS}]$	(3.2)
	$\text{TOT}_{\text{H}_2} = [\text{H}_2(\text{aq})] + \frac{1}{2}([\text{Fe}^{2+}] + [=\text{FeOFe}^{(II)+}] + [\text{DMRB}-\text{Fe}^{2+}]) + [\text{AH}_2\text{DS}]$	(3.3)
	$\text{TOT}_{\text{H}^+} = [\text{H}^+] + [=\text{FeOH}_2^+] - [=\text{FeO}^-] + [=\text{FeOFe}^{(II)+}] + [\text{HPIPES}] + 2([\text{Fe}^{2+}] + [\text{DMRB}-\text{Fe}^{2+}])$	(3.4)
	$\text{TOT}_{\text{DMRB}} = [\text{DMRB}] + [\text{DMRB}-\text{Fe}^{2+}]$	(3.5)
	$\text{TOT}_{\text{PIPES}} = [\text{PIPES}^-] + [\text{HPIPES}]$	(3.6)
Kinetic Reaction Rate Formulations		
	$R_1 = k_{\text{fss}}([=\text{FeOH}_2^+] + [=\text{FeOH}] + [=\text{FeO}^-])$	(4.1)
	$R_2 = k_2^{\text{f}}[\text{AQDS}][\text{DMRB}]$	(4.2a)
	$R_7 + R_8 + R_9 = k_{789}^{\text{f}}[=\text{FeO}^-][\text{Fe}^{2+}] - k_{789}^{\text{b}}[=\text{FeOFe}^{(II)+}]$	(4.3)

^A Refer to Eq. 1.2 in text for definition of terms.

In this manner a rate formulation can be proposed and rate parameters can be determined, and then the validity of the rate formulation can be tested under other experimental conditions.

The concentrations of all species were computed using Mathematica (Wolfram Research, Champaign, IL) based on N_K measured quantities, N_C mass conservation equations, and N_E mass action equations. Rate formulations were proposed and simulations of the reaction network were conducted to validate rate formulations and determine rate parameters using BIO-GEOCHEM, and compared with experimental data. Activity was used in mass action equations and for rate formulation purposes, and concentration was used in all mass conservation equations. The Davies equation was used to calculate activity coefficients for dissolved species, and the activity coefficient was set equal to 1 for solid phase species and adsorbed species. Surface electric field effects were not included in mass action or kinetic-variable equations involving solid phase species (i.e., Eqn. 1.3, 1.4, and 4.3) although they can be included in BIO-GEOCHEM. Surface electric field effects were not included because the pH remained constant (6.8) and the ionic strength remained near constant (50 mM PIPES) although a maximum dissolved concentration of ca. 0.6 mM Fe(II) was produced in some experiments. Concentrations were in mol L^{-1} including solid phase species. We have recently presented theoretical aspects related to reaction-based modeling (Yeh et al., 2001) and detailed step-by-step reaction-based modeling procedures for a subset of the biogeochemical system used here (Burgos et al., 2002).

3. EXPERIMENTAL METHODS

3.1. Microorganism and Culture Conditions

The dissimilatory iron-reducing bacterium *Shewanella putrefaciens* CN32 was provided from the Subsurface Microbial Culture Collection courtesy of Dr. David Balkwill (Florida State University). Details of methods for culturing and harvesting cells for inoculation have been described elsewhere (Royer et al., 2002). Harvested *S. putrefaciens* CN32 cells were resuspended in anaerobic 50 mM PIPES-30 μM phosphate buffer (pH=6.8, referred to as PIPES-phosphate buffer), and a final cell concentration of 10^8 cells mL^{-1} was added to the majority of experiments. Bacterial viability was measured by direct counts using the LIVE/DEAD BacLight™ viability stains (Molecular Probes, Eugene, OR) to determine the ratio of live to dead cells.

3.2. Materials

Hematite ($\alpha\text{-Fe}_2\text{O}_3$) from J.T. Baker (Phillipsburg, NJ) had a specific surface area of $9.04 \text{ m}^2 \text{ g}^{-1}$ measured by 5-point BET- N_2 adsorption. Mössbauer spectroscopy and X-ray diffraction did not reveal any impurities. Hematite suspensions were prepared in anaerobic PIPES-phosphate buffer at least 24 h before use to allow for complete surface hydration. Anthraquinone-2,6-disulfonate (AQDS, Sigma-Aldrich, St. Louis, MO) was used as received and a 9.94 mM filtered (0.2 μm) stock solution was prepared in PIPES-phosphate buffer.

3.3. Analytical Techniques

In the various kinetic experiments the following parameters were routinely measured or recorded: dissolved Fe(II), total Fe(II), total Fe, AH_2DS , total AQDS, pH, $\text{H}_2(\text{g})$ and temperature. Dissolved Fe(II) was measured by ferrozine with filtered (0.2 μm) sample aliquots (Burgos et al., 2002). Total Fe(II) was measured by ferrozine after 24 h extraction in 0.5 N HCl and filtration (0.2 μm). Total Fe was measured by ferrozine after extraction in 0.5 N HCl along with 0.5 g sodium dithionite/20–50 mg hematite. For samples with *S. putrefaciens* CN32 and hematite, several additions of dithionite over several days were

required to obtain a final constant value. AH_2DS was measured by absorbance at 405 nm with an Ocean Optics (Dunedin, FL) Palm-SPEC spectrophotometer placed within the anaerobic chamber on unacidified, filtered (0.2 μm) sample aliquots. Total AQDS was measured by absorbance at 405 nm on unacidified, filtered (0.2 μm) sample aliquots spiked with excess sodium dithionite to reduce all AQDS. AH_2DS concentrations were corrected for background absorbance by AQDS (and dithionite when appropriate). Solution pH was determined by combination electrode on sample filtrate in the anaerobic chamber. $\text{H}_2(\text{g})$ concentrations were recorded from the Coy gas meter (Grass Lake, MI) in the anaerobic chamber. In all experiments the $\text{H}_2(\text{g})$ concentration remained constant over the duration of each experiment and was 2.5–2.8% of the chamber atmosphere (remainder was N_2). Temperature was recorded from a digital thermometer in the anaerobic chamber. All experiments were performed in a 20°C constant temperature room.

3.4. Fe(II) Sorption to Hematite

Previously described experimental methods (Jeon et al., 2001) were used to measure the sorption of 0.125 or 0.25 mM Fe(II) (added as acidified FeCl_2) to 2.0 g L^{-1} of hematite in PIPES-phosphate buffer. At various times, triplicate samples were collected and analyzed for dissolved Fe(II), total Fe(II), total Fe and pH.

3.5. Biologic Reduction of AQDS

The bioreduction of AQDS was measured in serum bottles sealed with Teflon-faced butyl rubber stoppers and aluminum crimp tops. The atmosphere within the bottles was maintained at a near-constant concentration of $\text{H}_2(\text{g})$ by adding oxygen-free N_2/H_2 gas mix (97.5/2.5%) after sample collection. $\text{H}_2(\text{aq})$ was provided as the sole electron donor. All experiments were prepared in PIPES-phosphate buffer, and all bottle contents were magnetically stirred at ca. 400 rpm. The following combinations of AQDS and cell concentrations, respectively, were tested: 50 μM with 10^8 cells mL^{-1} ; 50 μM with 5×10^7 cells mL^{-1} ; and 140 μM with 10^8 cells mL^{-1} . Time-course samples were collected to measure AH_2DS , total AQDS and pH. All experiments were replicated three times. No AH_2DS was ever detected in uninoculated controls and in controls with cells amended with 20 mM NaN_3 (prepared in quadruplicate and sampled once after 120 min).

3.6. Chemical Reduction of Hematite by AH_2DS

AQDS solutions (500 μM) were incubated for 72 h with *S. putrefaciens* CN32 (10^8 cells mL^{-1}) in PIPES-phosphate buffer to biologically produce AH_2DS in crimp sealed 120 mL serum bottles. The AH_2DS solutions were autoclaved and filtered (0.2 μm) before being used in two types of experiments. In the first experiment, 125 μM AH_2DS was reacted with sterile hematite (2.0 g L^{-1}), sterile Fe(III)-citrate (ca. 0.75 mM) or a sterile Fe(III)-free blank. Samples were analyzed after 24 h for AH_2DS , pH, and total Fe(II). In the second experiment, 50 μM AH_2DS was reacted with sterile hematite (2.0 g L^{-1}) and samples were collected as quickly as possible (ca. 1.5 min and at 4 min) to measure AH_2DS and pH. The first experiment was replicated three times and the second experiment was replicated four times. In both types of experiments Fe(II) was measured with 1,10-phenanthroline (APHA, 1995) modified using NH_4F (Jeon et al., 2001).

3.7. Bioreduction of Hematite-with-AQDS

Hematite-with-AQDS bioreduction experiments were conducted in serum bottles using 2.0 g L^{-1} hematite ($0.0125 \text{ mol Fe}_2\text{O}_3 \text{ L}^{-1}$) with 50 μM AQDS and 10^8 cells mL^{-1} in PIPES-phosphate buffer (Royer et al., 2002). Bottles were sealed with Teflon-faced butyl rubber stoppers and aluminum crimp tops, and all bottle contents were magnetically stirred at ca. 400 rpm. Time-course samples were collected to measure dissolved Fe(II), total Fe(II), total Fe, AH_2DS , total AQDS and pH, and to record $\text{H}_2(\text{g})$. The atmosphere within the bottles was maintained at a near-constant concentration of $\text{H}_2(\text{g})$ by adding oxygen-free N_2/H_2 gas mix (97.5/2.5%) after sample collection. Triplicate samples were collected for each sampling event and the experiment was replicated four times. AQDS-free inoculated (biotic) controls were

run in parallel with all replicates. No Fe(II) was ever detected in uninoculated controls and in controls with cells amended with 20 mM NaN_3 . Abiotic controls were prepared with and without AQDS, in quintuplicate, and sampled once after 24 or 120 h.

4. RESULTS

4.1. Reaction Matrix Decompositions

The reaction network for the hematite-with-AQDS bioreduction experiments is summarized in Table 1. The network includes 14 species ($M = 14$), 11 reactions ($N = 11$), six of which were considered equilibrium reactions ($N_E = 6$) and eight of which are independent reactions ($N_I = 8$), and six chemical components ($N_C = M - N_I = 6$). Based on literature, we have assumed that the hematite surface hydration (R4), hematite surface acidity (R5, R6) and PIPES buffering (R11) reactions are fast reactions that can be considered at equilibrium. We have experimentally determined that the chemical reduction of hematite by AH_2DS (R3) (current study) and Fe(II) biosorption to DMRB (R10) (Burgos et al., 2002) are also fast reactions that can be considered at equilibrium. Experiments were designed to yield the simplest reaction network with the fewest chemical species (Yeh et al., 2001; Burgos et al., 2002). Most of the proposed reactions are not likely to be elementary reactions, and a series of one-step elementary reactions would need to be proposed to simulate the various reaction mechanisms. A greater understanding of the reactions would be required, and a correspondingly greater amount of measured experimental quantities would be required to simulate the larger, more complicated reaction network.

In numerical modeling of reaction-based biogeochemical processes, the evolution of M chemical species can be described by the principle of chemical kinetics as follows (Stumm and Morgan, 1996):

$$\frac{dC_i}{dt} = \sum_{k=1}^N (\nu_{ik} - \mu_{ik}) R_k, \quad i \in M \quad (5)$$

where C_i is the concentration of the i -th chemical species, N is the number of chemical reactions (both equilibrium and kinetic), ν_{ik} is the reaction stoichiometry of the i -th species in the k -th reaction associated with the products, μ_{ik} is the reaction stoichiometry of the i -th species in the k -th reaction associated with the reactants, R_k is the rate of the k -th reaction. In matrix form, Eqn. 5 can be stated as:

$$\mathbf{U} \frac{d\mathbf{C}}{dt} = \mathbf{\nu} \mathbf{R} \quad (6)$$

where \mathbf{U} is a unit matrix, \mathbf{C} is a column vector with M species concentrations, $\mathbf{\nu}$ is the reaction stoichiometry matrix, and \mathbf{R} is a column vector with N reaction rates. According to Eqn. 5 for the reaction matrix shown in Table 1, 14 simultaneous ordinary differential equations (ODEs) would have to be solved to simulate the production-consumption of the 14 chemical species concentrations (i.e., 14 unknowns). An analytical solution of Eqn. 5 is rarely possible and numerical integration encounters several difficulties, discussed below in section 5. The diagonalization-decomposition procedure will first reduce the number of ODEs by the number of mass conserved chemical

components (N_C). In other words, the original set ODEs (Eqn. 5 or Eqn. 6) is replaced by N_C linear algebraic equations and $(M - N_C)$ ODEs. These $(M - N_C)$ ODEs govern the production-consumption of $(M - N_C)$ kinetic-variables. Hence, they are called kinetic-variable equations. This new set of equations is equivalent to the original M ODEs, each of which governs the production-consumption of a single chemical species.

The diagonalization-decomposition procedure will further reduce the number of kinetic-variable equations by the number of independent equilibrium reactions (N_E). If a reaction is “fast” and reversible such that local equilibrium can be assumed, then its rate is conceptually infinite. The infinite rate of an equilibrium reaction is mathematically represented by a mass action equation or by a user-specified algebraic equation. When a fast reaction is represented by a mass equation, it can be used to eliminate one unknown and effectively replace a kinetic-variable equation. To make this elimination possible, the kinetic-variable equation which is to be replaced by a mass action equation should contain one and only one infinite rate. The diagonalization-decomposition preprocessor in BIOGEOCHEM will automatically achieve the task of rendering only one infinite rate (or none at all) in any differential equation governing a kinetic-variable. For example, using Eqn. 6 with the reaction matrix in Table 1, after diagonalization the following equation for the kinetic variable ($[=\text{FeOH}_2^+] + [=\text{FeOFe}^{(II)+}]$) would yield:

$$\frac{d([=\text{FeOH}_2^+] + [=\text{FeOFe}^{(II)+}])}{dt} = -R_5 + R_8 + R_9 \quad (7)$$

Based on our specified assumptions/measurements regarding equilibrium and kinetic reactions, only the rate of reaction R5 (denoted as R_5) is infinitely large (while reaction rates R_8 and R_9 are finite/slow). Because only R_5 in Eqn. 7 is infinite, Eqn. 7 can be replaced by $R_5 = \infty$, which is equivalent to stating that mass action Eqn. 1.3 can be used to replace kinetic-variable Eqn. 7, thereby reducing the number of kinetic-variables by one. All mass action equations shown in Tables 1 and 2 were determined in a similar manner.

The kinetic-variables, N_K (where $N_K = M - N_C - N_E$), following the diagonalization-decomposition procedure are all represented by independent, segregated equations. Thus, rate formulations can be proposed and rate parameters can be determined for the production-consumption of each kinetic-variable independent of all other reactions. For example, inspection of kinetic-variable Eqn. 8 in Table 2 reveals that the concentration of AH_2DS -versus-time (directly measured during these experiments) can be used to evaluate R2. Inspection of kinetic-variable Eqn. 2.1 in Table 1 reveals that the relative contributions of R1 and R2 to biogenic Fe(II) production cannot be segregated. In previous hematite-only bioreduction experiments the corresponding kinetic-variable equation was (Burgos et al., 2002):

$$\frac{1}{2} \frac{d([[\text{Fe}^{2+}] + [=\text{FeOFe}^{(II)+}] + [\text{DMRB} - \text{Fe}^{2+}])}{dt} = R_1 \quad (10)$$

thus, rate formulations/parameters could be determined for R1 independent of all other reactions. Furthermore, the rate formulations/parameters for R1 were based on direct measure-

Table 2. Reaction network, matrix decomposition and reaction-based rate formulations for the bioreduction of AQDS.

Reaction	Reaction Number	Reaction Parameters
Bacterial Reduction of AQDS $AQDS + H_2(aq) \rightleftharpoons AH_2DS$	(R2)	Eq. 4.2
PIPES Buffering $HPIPES \rightleftharpoons PIPES + H^+$	(R11)	$\log K_{11}^c = -6.80$
N_E Mass Action Equations	$K_{11}^e = \frac{[PIPES^-][H^+]}{[HPIPES]}$	(1.6)
$(N_I - N_E)$ Kinetic-Variable Equation	$\frac{d[AH_2DS]}{dt} = R_2$	(8)
N_C Mass Conservation Equations	$TOT_{AQDS} = [AQDS] + [AH_2DS]$	(3.2)
	$TOT_{PIPES} = [PIPES^-] + [HPIPES]$	(3.6)
	$TOT_{H_2} = [H_2(aq)] + [AH_2DS]$	(9.1)
	$TOT_{H^+} = [H^+] + [HPIPES]$	(9.2)
Kinetic Reaction Rate Formulation	$R_2 = k_2^f[AQDS][DMRB]$	(4.2a)
	$R_2 = \frac{V_{max}[AQDS]}{K_M + [AQDS]}$	(4.2b)

ments since the left-hand side of the Eqn. 10 was assumed to equal total Fe(II) [i.e., 0.5 N HCl extractable Fe(II)].

Inspection of kinetic-variable Eqn. 2.2 in Table 1 reveals that the concentration of hematite-sorbed Fe(II) (designated as $=FeOFe^{(II)+}$) could be used to evaluate the sorption of Fe(II) to hematite (represented by the lumped kinetic reactions R7 + R8 + R9). However, in these bioreduction experiments the left-hand side of Eqn. 2.2 could not be operationally isolated due to biosorption of Fe(II) to DMRB (R10). Previously, a reaction-based rate formulation for Eqn. 2.2 was obtained from experiments that measured the kinetics of abiotic sorption of Fe(II) to hematite (Eqn. 4.3, Table 1; Burgos et al., 2002). In those experiments the DMRB- Fe^{2+} species was not present and the difference between total Fe(II) and dissolved Fe(II) was operationally defined to equal $=FeOFe^{(II)+}$. Thus, for the evaluation of kinetic reactions it is important that the kinetic-variable (single species concentration or operational quantity) can be directly measured and that only one reaction contributes to its production-consumption (or several reactions for lumped kinetic reactions).

For the decomposition shown in Table 1, the relative contributions of bacterial reduction of hematite (R1) and bacterial reduction of AQDS (R2) leading to reduction of hematite by AH_2DS (R3) could not be segregated. To uniquely segregate the contribution of the parallel reactions R1 and R2+R3, a series of separate kinetic experiments were performed (Fig. 1). Individual experiments were designed such that only one significant kinetic reaction was operative at a time. The bioreduction kinetics of hematite (without AQDS) were measured previously (Burgos et al., 2002) and an empirical rate formulation adequately simulated R1 (Eqn. 4.1, Table 1). The empirical rate formulation was proposed to be first-order with respect to

hematite "free" surface sites [i.e., surface hydroxyl sites unoccupied by Fe(II)] (Roden and Urrutia, 1999; Liu et al., 2001a). Hydrogen was not included in the rate formulation because $[H_2(aq)]$ in these experiments was orders of magnitude greater than K_M values reported for hydrogen for DMRB (Lovley and Goodwin, 1988) (i.e., system was never electron donor-limited). In our experiments the rate and extent of hematite bioreduction was not effected when experiments were conducted at $H_2(g)$ concentrations of 2.5% and 5.0%. The concentration of DMRB was not included in the rate formulation. Stone (2002) and Roden and Zachara (1996) have reported that the rates of hematite and goethite bioreduction, respectively, were not proportional to the DMRB concentration. Unlike liquid culture systems with soluble electron acceptor(s) and electron donor(s), the presumption that all cells will be equally "active" in a system with a solid-phase electron acceptor is suspect because of limited sites for bacterial attachment to the oxide. Bacterial viability, however, remained between 93 to 99% after 5 d of incubation as measured by direct counts using the LIVE/DEAD *Ba*light viability stains (Molecular Probes, Eugene, OR). Since we do not yet know how solid-phase ferric oxide bioreduction rates vary as a function of DMRB concentration, inclusion of DMRB concentration is not possible at this time.

We have previously reported that there was no statistical difference between hematite bioreduction in the presence or absence of 30 μM phosphate (Burgos et al., 2002). While phosphate could participate in a number of reactions (e.g., vivianite precipitation, phosphate sorption to hematite, Fe(II) complexation with phosphate), these results suggest that phosphate played no significant role in these experiments. Furthermore, based on surface complexation constants for phosphate adsorption onto hematite (in MINTEQA6 from Dzombak and Morel,

1990), 0.1 μM of the 30 μM total would remain in solution. Based on a maximum dissolved phosphate concentration of 0.1 μM , and a maximum dissolved concentration of 0.6 mM Fe(II) (e.g., see Fig. 6), vivianite formation would never occur in these experiments. It should be noted that only the sorption of divalent cations was assumed to consume “free surface sites” and that sorption of all other counter- and co-ions was assumed to have no effect on the rate of bioreduction.

The decomposition shown in Table 1 is based on the selection of Fe_2O_3 , AQDS, H_2 , H^+ , DMRB and PIPES as component species, corresponding to mass conservation Eqn. 3.1–3.6, respectively. Eqn. 3.1 defines $\text{TOT}_{\text{Fe}_2\text{O}_3}$ as the total concentration of both Fe(II) and Fe(III) species. The $=\text{FeOFe}^{(\text{II})+}$ species accounts for two moles of iron, one on the hematite surface (i.e., $=\text{FeO}-$) and one sorbed to hematite (i.e., $-\text{Fe}^{(\text{II})+}$). Since $\text{H}_2(\text{aq})$ was replenished during these experiments, Eqn. 3.3 is decoupled from the system and used to account for the total amount of component mass that must be replenished to the system to maintain a constant concentration of $\text{H}_2(\text{aq})$.

The reaction network for the bioreduction of AQDS, its decomposition and kinetic rate formulations are presented in Table 2. Mass conservation Eqn. 3.2 was used to validate partial system consistency for this system. Reaction-based rate formulations could be obtained for kinetic-variable Eqn. 8 because the left-side of this equation was directly measured. An empirical and a Monod rate formulation (Eqn. 4.2a and 4.2b, respectively) were tested to simulate R2.

4.2. Surface Sites and Equilibrium Reactions

Preliminary experiments or literature references were used to determine all equilibrium reaction constants (R3–R6, R10, R11). The value of the equilibrium constant for the chemical reduction of hematite by AH_2DS (R3) used in these simulations is discussed in detail below. For the surface hydration reaction (R4), the following user-specified algebraic equation (rather than the mass action equation based on the stoichiometry of R4) was used (Burgos et al., 2002):

$$K_4^c[\text{Fe}_2\text{O}_3] = [= \text{FeOH}]_T \\ = [= \text{FeOH}_2^+] + [= \text{FeOH}] + [= \text{FeO}^-] + [= \text{FeOFe}^{(\text{II})+}]$$

$$\text{where } K_4^c = \frac{S_A N_S}{N_A} \text{MW}_{\text{Fe}_2\text{O}_3} \quad (1.2)$$

where $[\text{Fe}_2\text{O}_3]$ is the hematite suspension concentration (mol L^{-1}), $[= \text{FeOH}]_T$ is the total hematite surface site concentration (mol sites L^{-1}), K_4^c is the equilibrium constant for R4, S_A is the hematite unit surface area ($\text{m}^2 \text{g}^{-1}$), N_S is the surface site density (mol sites m^{-2}), N_A is Avagadro’s number (mol sites mol^{-1}), and $\text{MW}_{\text{Fe}_2\text{O}_3}$ is the molecular weight of hematite (g mol^{-1}) (Stumm and Morgan, 1996). This equation specifies that the concentration of hematite surface sites is proportional to the total hematite suspension concentration. The site density of 5.1 sites nm^{-2} was based on sorption isotherm data for Fe(II) to hematite (Jeon et al., 2001). Less than 4% of the hematite was bioreduced in these experiments, and therefore the use of algorithms such as a “shrinking sphere” geometric model (Yeh et al., 2001) to account for hypothetical changes in surface area was unnecessary.

A near-constant partial pressure of $\text{H}_2(\text{g})$ was maintained in the serum bottles during these experiments. The activity of $\text{H}_2(\text{aq})$ was assumed to be constant during all experiments since the half-time for mass transfer of $\text{H}_2(\text{g})$ across the gas-water interface was ca. 1 min. All serum bottle contents were magnetically mixed at ca. 400 rpm to eliminate H_2 transfer diffusion effects. Experiments performed with Fe(III)-citrate at these same $\text{H}_2(\text{g})$ concentrations maintained significantly greater $\text{H}_2(\text{aq})$ utilization rates suggesting that the dissolution of $\text{H}_2(\text{g})$ would never become rate-limiting in the hematite experiments. Therefore, the equilibrium reaction for the dissolution of $\text{H}_2(\text{g})$ was not included in the reaction matrix (as it would be redundant to setting the $[\text{H}_2(\text{aq})]$).

The equilibrium surface acidity constants for hematite were assumed to equal -7.31 and -8.93 for $\log K_5^c$ and $\log K_6^c$, respectively (Dzombak and Morel, 1990). The equilibrium constant for Fe(II) sorption to *S. putrefaciens* CN32 ($\log K_{10}^c = +1.43$) was previously determined (Burgos et al., 2002). The equilibrium constant for PIPES buffering ($\log K_{11}^c = -6.80$) was based on product information (Sigma-Aldrich, St. Louis, MO).

4.3. Sorption of Fe(II) to Hematite

In previous experiments (Burgos et al., 2002), 0.18 mM Fe(II) was reacted with 2.0 g $\text{Fe}_2\text{O}_3 \text{L}^{-1}$ at pH 6.8 ± 0.2 in PIPES-phosphate buffer. An elementary rate formulation for the lumped kinetic reactions R7 + R8 + R9 (Eqn. 4.3, Table 1) fit the previous data well. To further test this rate formulation before using it again in the current study, additional experiments were performed with 0.125 and 0.25 mM Fe(II) under otherwise identical conditions. The previously estimated rate parameters over-predicted the rate and extent of Fe(II) sorption (simulations not shown). Therefore, new elementary rate parameters were independently estimated for each experiment. Updated estimates averaged from the four simulations (two previous, two current) were then used to simulate R7 + R8 + R9 for all remaining simulations.

For two of the four simulations with the updated-averaged parameters, the fits were poor for the abiotic sorption of Fe(II) to hematite (Table 3). These simulations were very sensitive to the initial conditions specified in the model. However, the updated-averaged parameters were used in all other bioreduction simulations because they were based on more experimental observations. The elementary rate formulation/parameters adequately predicted the distribution of Fe(II) between dissolved and sorbed species in the hematite-only (Fig. 2) and in the hematite-with-AQDS bioreduction experiments (Figs. 5 and 6).

4.4. Sorption of Fe(II) to *S. putrefaciens* CN32

The sorption of Fe(II) to *S. putrefaciens* CN32 has recently been reported by Liu et al. (2001b) and Burgos et al. (2002). In the sorption experiments performed by Liu et al. (2001b), cell concentrations ranged from 7×10^7 to 5×10^8 cells mL^{-1} and Fe(II) concentrations ranged from 0.01 to 6.0 mM at pH 7.0 in 30 mM PIPES solution with no phosphate. Biosorption equilibrium was attained in less than 30 min and suspensions were reacted for 24 h. The biosorption data was well fit by the Langmuir isotherm equation shown in Table 4. In the sorption

Table 3. Summary of elementary reaction rate parameters for the abiotic sorption of Fe(II) to hematite (R7+R8+R9), and R² values.

Rate Parameters	Experimental Conditions and Corresponding Independently Obtained Parameter Values				Updated-Averaged Parameter Values
	Fe(II) = 0.18 mM pH = 6.62 ^A	Fe(II) = 0.18 mM pH = 6.84 ^A	Fe(II) = 0.25 mM pH = 6.80	Fe(II) = 0.125 mM pH = 6.80	
$\log k_{789}^f (\text{M}^{-1} \text{hr}^{-1})$	6.94	6.37	5.84	7.02	6.54
$\log k_{789}^b (\text{hr}^{-1})$	0.47	0.19	-0.30	0.78	0.28
$\log(k_{789}^f/k_{789}^b)$	6.47	6.19	6.14	6.24	
R ² with independent parameters	0.972	0.820	0.854	0.722	
R ² with updated-averaged parameters	-1.61	0.811	-0.577	0.982	

^A Results previously reported by Burgos et al. (2002).

experiments performed by Burgos et al. (2002), the cell concentration was a constant 10^8 cells mL^{-1} and Fe(II) concentrations ranged from 0.09 to 0.22 mM at pH 6.8 in 50 mM PIPES-30 μM phosphate solution. Biosorption equilibrium was attained in less than 5 min and suspensions were reacted for 24 h. A linear sorption isotherm was used to fit the data (Eqn. 1.5, Table 1), and this equilibrium expression was used for the previous simulation of hematite-only bioreduction experiments. The amount of Fe(II) biosorption to *S. putrefaciens* CN32 reported by Burgos et al. (2002) was lower by a factor of 2.93 to 1.11 compared to Liu et al. (2001b) at soluble Fe(II) concentrations of 0.02 to 0.90 mM, respectively (range observed in current study). [Previously we erroneously reported that these two equilibrium expressions differed by a factor of ca. 600 (Burgos et al., 2002).]

To test the sensitivity of hematite-only bioreduction simulations to Fe(II) biosorption, the two equilibrium expressions for R10 (Table 4) were compared while holding all other rate formulations/parameters constant. Model predictions of total and dissolved biogenic Fe(II) were relatively insensitive to the equilibrium expression for R10 (Fig. 2). The distribution of biogenic Fe(II) between the dissolved and sorbed species was also insensitive to the equilibrium expression for R10. Because the R² values (Table 4) were not substantially effected or improved using the Langmuir isotherm, we retained our linear

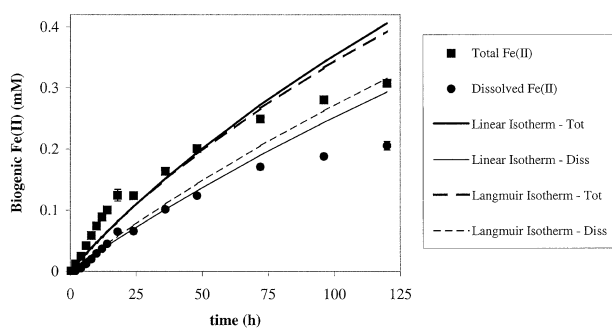


Fig. 2. Effect of the equilibrium expression for biosorption of Fe(II) to *S. putrefaciens* CN32 on model simulations of the biologic reduction of hematite-only. Experimental data are shown as symbols, error bars represent standard deviation of triplicate measurements, and model results are shown as lines. A linear sorption isotherm reported by Burgos et al. (2002) is compared to a Langmuir sorption isotherm reported by Liu et al. (2001b).

isotherm and our previously reported equilibrium constant for all remaining simulations. The overprediction of Fe(II) concentrations at later time points (e.g., >72 h) may have been caused by the decreased thermodynamic potential for further iron reduction (i.e., rate decreases due to product accumulation).

The two proposed biosorption equilibrium expressions are only applicable to the limited experimental conditions under which they were obtained (i.e., specified pH and ionic strength). The adsorption-desorption of metals to bacterial surfaces can be modeled as a series of surface complexation reactions to different cell wall functional groups such as carboxylate, phosphate and phenolate groups (Fein et al., 1997). A bacterial surface complexation approach would thus replace R10 with a series of reactions that would then be applicable to other pH conditions. While this would be advantageous, additional experiments would be required to determine the requisite reaction constants.

4.5. Biologic Reduction of AQDS

The bioreduction kinetics of AQDS are shown in Figure 3. Three separate experimental conditions were used to test two different rate formulations (Eqn. 4.2a,b, Table 2). All experiments were conducted in PIPES-phosphate buffer (pH 6.8) under a 2.5% H₂ atmosphere. One experiment was conducted with 50 μM AQDS and 10^8 cells mL^{-1} , one with 50 μM AQDS and 5×10^7 cells mL^{-1} , and one with 140 μM AQDS and 10^8 cells mL^{-1} . For each replicate (three per experiment, nine total), rate parameters for Eqn. 4.2a,b were independently determined. An empirical rate formulation was proposed to be first-order with respect to AQDS and first-order with respect to DMRB (Eqn. 4.2a). A cell concentration of 10^8 cells mL^{-1} was approximated as 0.005 mol cells L^{-1} based on a molecular formula of C₅H₇O₂N and a unit mass of 5×10^{-12} g cell⁻¹ (Burgos et al., 2002). The first-order rate formulation (Eqn. 4.2a) was selected for use in the subsequent simulations of the hematite-with-AQDS bioreduction experiments because it adequately fit the experimental data and because the estimates for the rate parameter k_2^F were consistent between the experiments. For the 50 μM AQDS- 10^8 cells mL^{-1} experiment, k_2^F was estimated to equal 1.12 ± 0.12 mol/L⁻¹ h⁻¹ (mean \pm sd, n=3). For the 50 μM AQDS- 5×10^7 cells mL^{-1} experiment and k_2^F was estimated to equal 1.01 ± 0.13 mol/L⁻¹ h⁻¹ (n=3). For the 140 μM AQDS- 10^8 cells mL^{-1} experiment, k_2^F was

Table 4. Summary of equilibrium expressions tested to simulate Fe(II) biosorption to *S. putrefaciens* CN32, and R² values. Excluding comparative results shown in Figure 2, the linear isotherm (mass action Eq. 1.5a) was used for all simulations of the hematite-with-AQDS bioreduction experiments.

	Linear isotherm ^A	Langmuir isotherm ^B
equation	$[\text{DMRB} - \text{Fe}^{2+}] = K_{10}^e [\text{DMRB}] [\text{Fe}^{2+}]$	$q = \frac{Q_{\max} [\text{Fe}^{2+} (2.5a)]}{b + [\text{Fe}^{2+}]}$
constants	$K_{10}^e = 26.8 (\text{mol cells})^{-1} \text{L}$	q reported in mol Fe(II)/10 ¹² cells Q _{max} = 4.19 mmol Fe(II)/10 ¹² cells b = 0.514 mmol Fe(II)
R ² for diss. Fe(II) with Eq. 4.1	$[\text{DMRB}] = 10^{11} \text{ cells L}^{-1} = 0.005 \text{ mol cells L}^{-1}$ 0.834	$[\text{DMRB}] = 10^{11} \text{ cells L}^{-1} = 0.005 \text{ mol cells L}^{-1}$ 0.716
R ² for total Fe(II) with Eq. 4.1	0.851	0.876

^A Reported by Burgos et al. (2002).

^B Reported by Liu et al. (2001b).

estimated to equal $1.20 \pm 0.22 \text{ mol/L}^{-1} \text{ h}^{-1}$ (n=3). A Monod rate formulation was proposed to be dependent on AQDS and not dependent on H₂(aq) (excess donor) or DMRB (Eqn. 4.2b). The Monod rate formulation was rejected because the estimates of K_M and V_{max} were highly variable amongst the replicates.

4.6. Chemical Reduction of Hematite by AH₂DS

The chemical reduction of hematite by AH₂DS was shown to be a “fast” equilibrium reaction. Within 1.5 to 4 min, 50 μM AH₂DS was completely oxidized to AQDS in a 2.0 g Fe₂O₃ L⁻¹ suspension at pH 6.8 in PIPES-phosphate buffer. In separate experiments, 125 μM AH₂DS was completely oxidized in a hematite suspension after 24 h. The corresponding measurement of total Fe(II) was $263 \pm 16 \text{ μM}$ (n=3) demonstrating near-stoichiometric production of Fe(II) from AH₂DS. Overproduction of Fe(II) (i.e., 263 vs. 250 μM) could have been caused by the presence of extracellular diffusible quinones produced by *S. putrefaciens* spp. (Newman and Kolter, 2000).

4.7. Biologic Reduction of Hematite-with-AQDS

Previous experiments were used to test kinetic rate formulations and obtain associated rate parameters for the biologic reduction of hematite by *S. putrefaciens* CN32 (Burgos et al., 2002). Experimental data was well simulated using the empirical first-order “free” surface sites rate formulation for hematite bioreduction (Eqn. 4.1, Table 1). The rate parameter was optimized using BIOGEOCHEM for four replicate experiments and the average value for k_{fss} was $0.018 \pm 0.0083 \text{ (h}^{-1}\text{)}$ (mean ± sd, n=4) with values ranging from 0.011 to 0.030 h⁻¹. Stone et al. (2002) conducted a series of hematite bioreduction kinetics experiments using variable concentrations of hematite (0.25 to 2.0 g L⁻¹) and variable concentrations of *S. putrefaciens* CN32 (10⁶ to 10⁸ cell mL⁻¹) in 10 mM PIPES buffer (pH 6.8). These experiments demonstrated that the rate of bioreduction was proportional to the hematite concentration (i.e., supports presumption that rate law is proportional to free surface sites) but was not proportional to the DMRB concentration (i.e., supports presumption that [DMRB] can not be easily incorporated into the rate law). Similar results were also reported by Roden and Zachara (1996) in experiments using 2.7×10^7 to

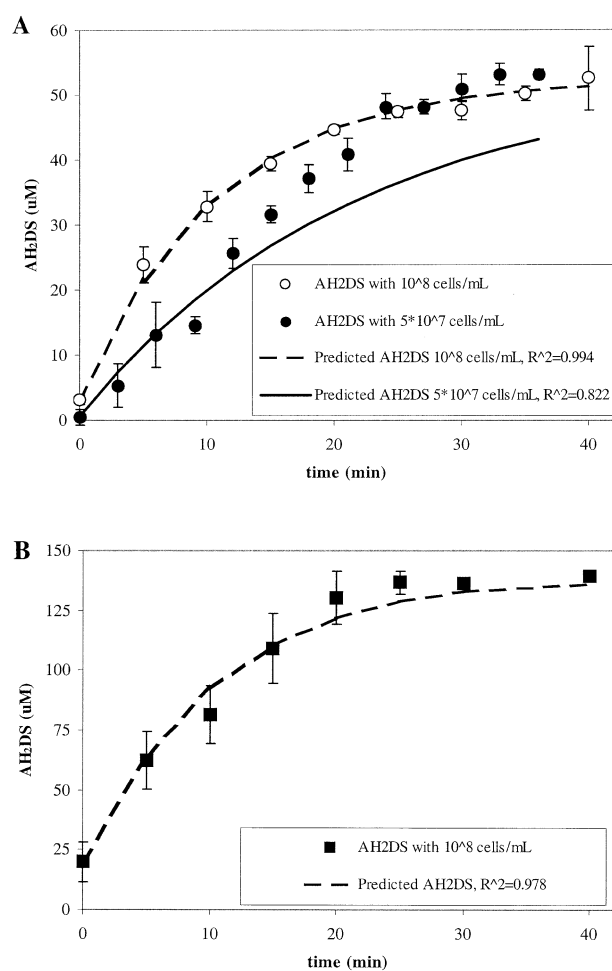


Fig. 3. Reaction kinetics for the biologic reduction of AQDS at pH 6.80 in 50 mM PIPES-30 μM phosphate buffer. A) 50 μM AQDS with 10⁸ cells mL⁻¹ and 5 × 10⁷ cells mL⁻¹ *S. putrefaciens* CN32. B) 140 μM AQDS with 10⁸ cells mL⁻¹ *S. putrefaciens* CN32. Experimental data are shown as symbols, error bars represent standard deviation of triplicate measurements, and model results are shown as lines. AQDS bioreduction rate was first-order with respect to AQDS and DMRB (Eqn. 4.2a).

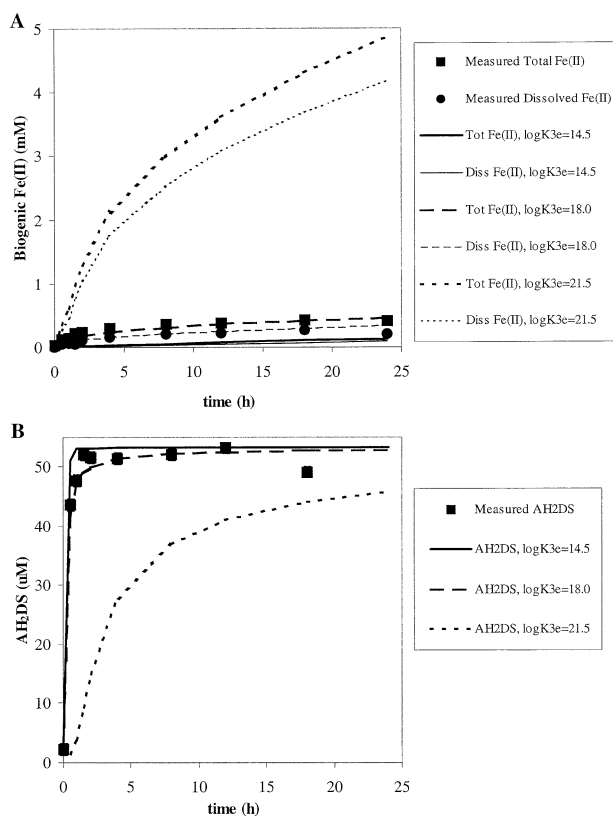


Fig. 4. Effect of $\log K_3^e$ (Eqn. 1.1) on model simulations of the biogenic reduction of hematite-with-AQDS—Experiment #1 (10^8 cells mL^{-1} *S. putrefaciens* CN32, 2.0 g $\text{Fe}_2\text{O}_3 \text{ L}^{-1}$, 50 mM PIPES-30 μM phosphate buffer). Production of A) biogenic Fe(II) and B) AH₂DS. Experimental data are shown as symbols, error bars represent standard deviation of triplicate measurements, and model results are shown as lines. Hematite bioreduction rate was first-order with respect to “free” surface sites (Eqn. 4.1). AQDS bioreduction rate was first-order with respect to AQDS and DMRB (Eqn. 4.2a).

2.2×10^9 cells mL^{-1} of *Shewanella alga* BrY and 20 mM amorphous Fe(III) oxide or 200 mM goethite in 10 mM PIPES buffer (pH 7.0).

The main objective of the “combined” parallel kinetics experiments (i.e., hematite-with-AQDS) was to validate the reaction-based modeling approach, i.e., demonstrate that the independently obtained “segregated” rate equations for R1, R2 and R7+R8+R9 and the assumed/determined equilibrium constants for R3-R6, R10 and R11 would simulate, without reformulation of rate equations and recalibration of rate parameters, the parallel kinetic reactions of Fe(II) production. For all sim-

ulations shown in Figures 4 to 6, the kinetic rate formulations and associated parameters are summarized in Table 5, and the equilibrium expressions and constants are included in Table 1. These simulations were shown to be quite sensitive to the value of the equilibrium constant for the chemical reduction of hematite by AH₂DS (R3) (Fig. 4). An equilibrium constant for R3 ($\log K_3^e$) can be calculated from standard state half cell potentials (E^0) for AH₂DS oxidation and ferric oxide reduction (Table 6). If hematite or amorphous ferric hydroxide (AFO, $\text{Fe}(\text{OH})_3$) are assumed as the ferric oxide phase, $\log K_3^{e\text{-theoretical}}$ can range from +14.5 to +32.1, respectively. Alternatively, a value for $\log K_3^e$ can be calculated using mass action Eqn. 1.1 (Table 1) and Mathematica (to calculate all species concentrations) at every time step for all four hematite-with-AQDS experiments. For example, for replicate Experiment #1, $\log K_3^e$ was calculated nine times (nine sampling events) and the average value was $\log K_3^e = 17.46 \pm 0.88$ (mean \pm sd, $n = 9$) with a minimum value of 16.02 and a maximum value of 18.82. Based on similar calculations from all four replicate experiments, the average value was $\log K_3^e = 18.03 \pm 0.85$ (mean \pm sd, $n=43$) with a minimum value of 15.75 and a maximum value of 19.43.

If $\log K_3^e$ was calculated assuming that hematite was being reduced by AH₂DS (i.e., $\log K_3^e = 14.5$), the model significantly under-predicted total and dissolved Fe(II) production, and predicted that AQDS would be reduced more quickly than it occurred (Fig. 4). An alternative value of $\log K_3^e = 21.5$ was used for demonstration purposes. This value of $\log K_3^e = 21.5$ was 3.5 orders of magnitude greater than the calculated average value of $\log K_3^e = 18.03$ that, in turn, was 3.5 orders of magnitude greater than the value for hematite. With a value of $\log K_3^e = 21.5$, the model significantly over-predicted total and dissolved Fe(II) production, and predicted that AQDS would be reduced more slowly and to a lesser extent than it occurred.

For these experiments, $\log K_3^e = 14.5$ simulated the data poorly (Fig. 4) while $\log K_3^e = 18.03$ simulated the data well (Figs. 5 and 6). The corresponding E^0 value for a ferric oxide participating in R3 with $\log K_3^e = 18.03$ would be +0.76 V, a value clearly intermediate between crystalline oxides (e.g., $\alpha\text{-Fe}_2\text{O}_3$ and $\alpha\text{-FeOOH}$) and AFO (Table 6). This result could imply that the hematite surface atoms have become more disordered upon hydration and, subsequently, their electrochemical properties have changed. There is some evidence to support this speculation. First, we have measured the bioreduction of hematite with quinones of varied reduction potentials and showed that methylene blue (MB) could stimulate bioreduction while 1,4-benzoquinone (BQ) could not (Royer et al., 2002). Based on standard state reduction potentials for MB, BQ and hematite, a quinone/hydroquinone ratio of 1/100, a $\text{Fe}^{2+}(\text{aq})$ concentration of 1 μM , and pH 6.8 (used to calculate

Table 5. Summary of kinetic reaction rate constants used for the simulation of hematite-with-AQDS experiments (Figures 4–6). All equilibrium expressions and constants are included in Table 1.

Reaction Number	Rate Formulation	Rate Parameters
R1	$R_1 = k_{\text{fss}}([\text{FeOH}_2^+] + [\text{FeOH}] + [\text{FeO}^-])$	$K_{\text{fss}} = 0.018 (\text{h}^{-1})$
R2	$R_2 = k_{\text{f}}^2[\text{AQDS}][\text{DMRB}]$	$k_{\text{f}}^2 = 1.11 (\text{M}^{-1} \text{h}^{-1})$
R7 + R8 + R9	$R_7 + R_8 + R_9 = k_{\text{f}}^{\text{f}}[\text{FeO}^-][\text{Fe}^{2+}] - k_{\text{b}}^{\text{f}}[\text{FeOFe}^{(\text{II})+}]$	$\log K_{\text{f}}^{\text{f}} = 6.54 (\text{M}^{-1} \text{h}^{-1})$ $\log k_{\text{b}}^{\text{f}} = 0.28 (\text{h}^{-1})$

Table 6. Reduction potentials of quinones and ferric oxides.

Half reaction ^a	E ⁰ (V)	E' (V) ^b	Source
$\frac{1}{2}\text{Q} + \text{H}^+ + \text{e}^- \rightleftharpoons \frac{1}{2}\text{HQ}$	+0.70	0.24	Fultz and Durst (1982)
$\frac{1}{2}\text{MB} + \text{H}^+ + \text{e}^- \rightleftharpoons \frac{1}{2}\text{HMB}$	+0.42	-0.04	Fultz and Durst (1982)
$\frac{1}{2}\text{AQDS} + \text{H}^+ + \text{e}^- \rightleftharpoons \frac{1}{2}\text{AH}_2\text{DS}$	+0.23	-0.23	Clark (1960)
$\text{Fe}(\text{OH})_3 + 3\text{H}^+ + \text{e}^- \rightleftharpoons \text{Fe}^{2+} + 3\text{H}_2\text{O}$	+0.95	+0.10	Stumm and Morgan (1996)
$\text{FeOOH} + 3\text{H}^+ + \text{e}^- \rightleftharpoons \text{Fe}^{2+} + 2\text{H}_2\text{O}$	+0.95	+0.10	Stumm and Morgan (1996)
$\alpha\text{-FeOOH} + 3\text{H}^+ + \text{e}^- \rightleftharpoons \text{Fe}^{2+} + 2\text{H}_2\text{O}$	+0.67	-0.18	Stumm and Morgan (1996)
$\frac{1}{2}\alpha\text{-Fe}_2\text{O}_3 + 3\text{H}^+ + \text{e}^- \rightleftharpoons \text{Fe}^{2+} + \frac{3}{2}\text{H}_2\text{O}$	+0.66	-0.19	Stumm and Morgan (1996)
$\text{H}^+ + \text{e}^- \rightleftharpoons \frac{1}{2}\text{H}_2(\text{aq})$	-0.09	-0.35	Stumm and Morgan (1996)

^a Q, HQ-1,4-benzoquinone and reduced form; MB, HMB-methylene blue and reduced form; AQDS, AH₂DS-anthraquinone-2,6-disulfonate and reduced form; Fe(OH)₃-ferric hydroxide (G_f⁰ = -699 kJmol⁻¹); FeOOH-amorphous ferric oxide (G_f⁰ = -462 kJmol⁻¹); α-FeOOH-goethite (G_f⁰ = -488.6 kJmol⁻¹); α-Fe₂O₃-hematite (G_f⁰ = -742.7 kJmol⁻¹); All G_f⁰ values from Stumm and Morgan (1996).

^b log [H⁺] = -6.8, [HQ] = 50 μM, [Q] = 0.50 μM, [Fe²⁺] = 1 μM, [H₂(g)] = 0.025 atm, 25°C.

E' values), neither reduced MB or BQ should have been re-oxidized by hematite (Table 6). Note that if a Fe²⁺(aq) concentration of 1 nM is assumed, reduced MB (HMB) could reduce hematite. However, for these specified E⁰ conditions the chemical reduction of hematite by HMB would proceed if E⁰ of the surface ferric atoms was > +0.81 mV, which corresponds

to log K₃^c = 19.7. Second, it has been reported that crystalline metal oxides react with water to form an external "shell" that is similar to hydrated hydroxy phases (Davis and Hem, 1989). Third, it has been reported that hematite becomes more disordered at its surface when immersed in water (Hansel, 2002) based on extended X-ray absorbance fine structure (EXAFS). Linear combination fits of hematite and 6-line ferrihydrite were used to examine hematite-coated sand in abiotic column experiments and showed that the 6-line ferrihydrite component increased by 20% after 16 d.

If a value of log K₃^c = 18.03 was used, the model adequately simulated the experimental results for both 24 h (Fig. 5) and 120 h experiments (Fig. 6). Replicate experiments were used to evaluate the consistency of the experimental results and corresponding model fits. The model simulations for Experiments #1 and #2 were essentially identical and only one simulation is shown in Figure 5 for clarity. The model simulations for Experiments #3 and #4 were also essentially identical. For Experiments #1 and #2, R² values were better for total Fe(II) compared to dissolved Fe(II) for the 24 h period (Fig. 5). As the length of the experiment and the corresponding simulation time increased, the R² values improved for both total and dissolved Fe(II) (Fig. 6). Because the bioreduction kinetics of AQDS were rapid, the R² values for AQDS were insensitive to simulation time and were consistently excellent (Figs. 5 and 6).

5. IMPLICATIONS FOR BIOGEOCHEMICAL MODELING

5.1. Advantages of Diagonalization-Decomposition Procedure

This is the first reported study where a diagonalized reaction-based model was used to simulate parallel kinetic reactions based on rate formulations/parameters independently obtained from segregated experiments. Others who have used reaction-based modeling have attempted to solve Eqn. 5, a set of simultaneous differential equations governing the production-consumption of all species, in its primitive form (Macquarrie et al., 1990; Lasaga, 1994; Lichtner and Seth, 1996; Soetaert et al., 1996; Xu et al., 1999; Liu et al., 2001a; Liu et al., 2002). Numerical integration of Eqn. 5 will encounter several major difficulties. First, the rates of N reactions can, in general, range over several orders of magnitude. If at least one of the reaction rates is orders of magnitude faster than the time-scale of inter-

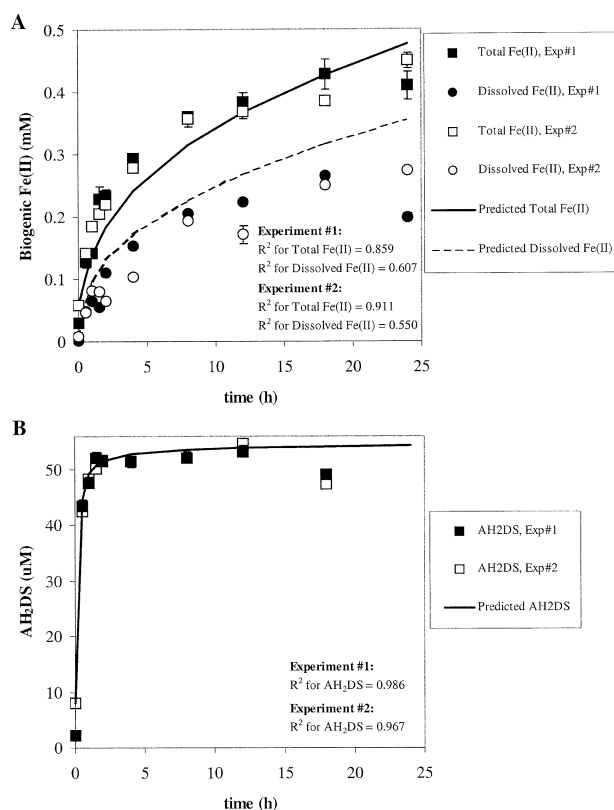


Fig. 5. One-day reaction kinetics for the biologic reduction of hematite-with-AQDS—Experiments #1 and #2 (10^8 cells mL⁻¹ *S. putrefaciens* CN32, 2.0 g Fe₂O₃ L⁻¹, 50 mM PIPES-30 μM phosphate buffer). Production of A) biogenic Fe(II) and B) AH₂DS. Experimental data are shown as symbols, error bars represent standard deviation of triplicate measurements, and model results are shown as lines. Hematite bioreduction rate was first-order with respect to "free" surface sites (Eqn. 4.1). AQDS bioreduction rate was first-order with respect to AQDS and DMRB (Eqn. 4.2a). For R3, log K₃^c = +18.03.

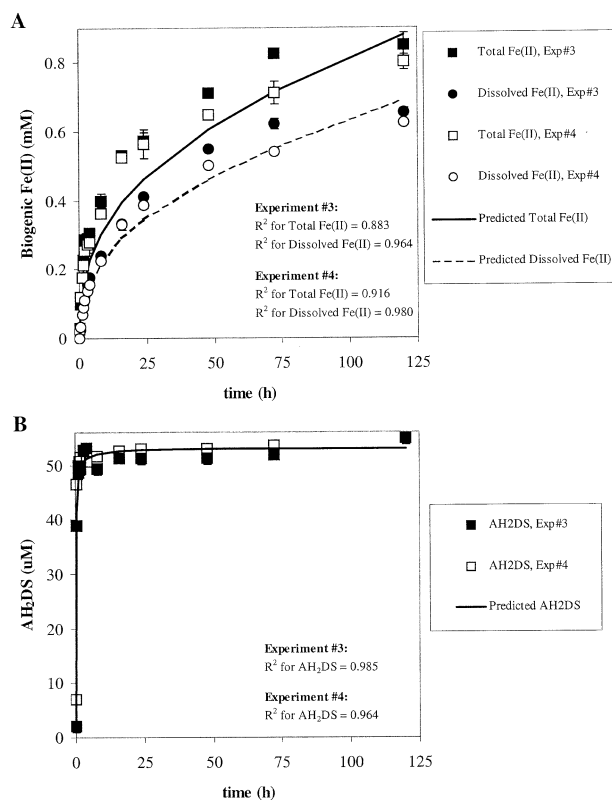


Fig. 6. Five-day reaction kinetics for the biologic reduction of hematite-with-AQDS—Experiments #3 and #4 (10^8 cells mL^{-1} *S. putrefaciens* CN32, $2.0 \text{ g Fe}_2\text{O}_3 \text{ L}^{-1}$, 50 mM PIPES - $30 \text{ }\mu\text{M}$ phosphate buffer). Production of A) biogenic Fe(II) and B) AH₂DS. Experimental data are shown as symbols, error bars represent standard deviation of triplicate measurements, and model results are shown as lines. Hematite bioreduction rate was first-order with respect to “free” surface sites (Eqn. 4.1). AQDS bioreduction rate was first-order with respect to AQDS and DMRB (Eqn. 4.2a). For R3, $\log K_3^s = +18.03$.

est, the time-step size must be extremely small relative to the time-scale of interest, which makes integration impractical. This difficulty can be alleviated with the mixed differential and algebraic equation (DAE) approach (e.g., Liu et al., 2001a) albeit with more computational demands (Yeh et al., 2002). However, the DAE approach will have difficulties overcoming the other difficulties described below (Fang et al., 2003). Second, for most practical problems the number of independent reactions is less than the number of species. This implies that there are one or more chemical components whose masses must be conserved during the reactions. For example, the diagonalization-decomposition shown in Table 1 explicitly enforces mass conservation of the six components using mass conservation Eqn. 3.1–3.6.

Third, a more severe problem of modeling directly with Eqn. 5 is that all reaction rates are coupled and, as a result, the segregation of kinetic reactions is extremely difficult if not impossible (Yeh et al., 2002). We have used, and recommend the use of, a matrix diagonalization-decomposition procedure (QR decomposition; Chen, 1994; Salvage and Yeh, 1998) to facilitate numerical integration of Eqn. 5. All reaction rates are decoupled through this procedure and kinetic reactions can easily be segregated (Yeh et al., 2001). Thus, matrix diagonal-

ization-decomposition determines the kinetic-variables and allows a rate formulation to be proposed for the associated kinetic reactions and rate parameters to be determined for each kinetic-variable independent of all other kinetic reactions (i.e., kinetic reactions are evaluated one reaction at a time).

Other advantages of the diagonalization-decomposition procedure include the automatic removal of redundant equilibrium reactions and irrelevant kinetic reactions (Fang, et al., 2003). Redundant equilibrium reactions must be removed from consideration, otherwise the system would become singular. Redundant equilibrium reactions can easily be detected and excluded from consideration manually when the system is simple and components are chosen a priori. However, when there are many reactions in the reaction network, redundancies are not easy to detect and a systemic way (such as the diagonalization procedure) must be employed for detection. Although the inclusion of irrelevant kinetic reactions will not pose computational difficulties, it will greatly increase computational burdens when there are many such reactions. More importantly, rate formulations/parameters for irrelevant kinetic reactions are meaningless because they are insensitive to the system. Because of this insensitivity, any rate formulation/parameter for irrelevant kinetic reactions can be used to calibrate model simulations to fit experimental results when using Eqn. 5. Therefore, as with redundant equilibrium reactions, a systemic approach should be used to detect and remove irrelevant kinetic reactions.

While the advantages of reaction-based modeling are significant there are also disadvantages. The primary disadvantage of using reaction-based modeling is that the proposition of the reaction network and the determination of reaction mechanisms are difficult. Reaction-based models with mechanistic rate formulations are admittedly ambitious and aim at representing the fundamental processes occurring in the system, and this will be extremely difficult in complex natural systems (Steeffel and van Cappellen, 1998). Another disadvantage is that the minimum data needs (i.e., measured experimental quantities) are much greater for reaction-based models compared to ad hoc models (Yeh et al., 2001). Another disadvantage of reaction-based modeling is that parallel kinetic reactions cannot be segregated. Therefore, as in this study, complex systems would have to be decomposed into simpler subsystems such that important rate formulations could be evaluated independently but would require a considerably greater amount of effort.

5.2. Experimental Validation

An empirical rate formulation for hematite bioreduction proposed to be first-order with respect to hematite “free” surface sites (Eqn. 4.1) adequately simulated the hematite-only experiments for the first ca. 72 h (Fig. 2) and the hematite-with-AQDS experiments for the complete 120 h (Figs. 5 and 6). Although this physically-based empirical rate formulation was adequate for the current study, our goal should be to elucidate the mechanism of biologic hematite reduction such that a series of one-step elementary reactions could be proposed (which would require more elaborate experiments to generate requisite data) and included in essentially any reaction network. Given that the foundations of diagonalized reaction-based modeling approaches have been laid (Yeh et al., 2001; Fang et al., 2003),

inclusion of mechanistic features should be the focus of future research.

For the bioreduction of AQDS (R2) an empirical first-order rate formulation (Eqn. 4.2a, Table 2) adequately simulated the experimental results (Fig. 3). The first-order rate formulation can be interpreted as a special case of the Monod rate formulation (Eqn. 4.2a) when the half-saturation constant (K_M) is much larger than the AQDS concentration. For these conditions ($K_M \gg [AQDS]$), the simultaneous optimization of V_{max} and K_M is very difficult and the highly variable estimates of these parameters from the replicate AQDS experiments may be due to numerical inaccuracies. Again, even though a first-order rate formulation was adequate for the current study, our goal should be to elucidate the mechanism of biologic AQDS reduction to most accurately simulate this process (i.e., using a larger number of elementary reactions) under varied conditions.

For the sorption of Fe(II) to hematite (R7 + R8 + R9) an elementary rate formulation (Eqn. 4.3) adequately simulated the reaction in isolation (Burgos et al., 2002) and simulated the distribution of biogenic Fe(II) in the hematite-only (Fig. 2) and the hematite-with-AQDS experiments (Figs. 5 and 6). An elementary rate formulation was adequate probably because the abiotic sorption of a divalent cation to a metal oxide could occur in one step. The variability in the rate parameters for the different experiments (Table 3) may reflect sorption to different site types (e.g., “strong” and “weak”; Dzombak and Morel, 1990) that were not included in our reaction network.

For the bioreduction of hematite-with-AQDS better R^2 values could likely have been achieved for each experiment if we tried the range of rate parameter values instead of the average values (Table 5). However, our goal was not to maximize the R^2 values via an optimization procedure. Instead, our goal was to demonstrate that parallel kinetic reactions can be resolved by the careful design of separate experiments to independently parameterize important reactions. These results suggest that complex biogeochemical systems which contain parallel kinetic reactions can be simulated using reaction-based models provided experiments are conducted to incrementally increase system complexity.

Acknowledgments—This research was supported by the Natural and Accelerated Bioremediation Research Program (NABIR), Office of Biologic and Environmental Research (OBER), U.S. Department of Energy (DOE) Grants No. DE-FG02-98ER62691 and No. DE-FG02-01ER63180 with the Pennsylvania State University. Dr. G.T. Yeh was also supported by the Biogeochemical Program, National Science Foundation (NSF) under Grant EAR-0196048 with the University of Central Florida. Dr. W.D. Burgos acknowledges support from the Cooperative Institute for Research in Environmental Sciences (CIRES) while on sabbatical at the University of Colorado at Boulder.

Associate editor: J. Fein

REFERENCES

- APHA (1995) Standard Methods for the Examination of Water and Wastewater (ed. A. P. H. Association), pp. 3–66 to 3–68 and 5–7 to 5–8.
- Brooks S. C., Carroll S. L., and Jardine P. M. (1999) Sustained bacterial reduction of Co(III)EDTA- in the presence of competing geochemical oxidation during dynamic flow. *Env. Sci. Tech.* **33**, 3002–3011.
- Burgos W. D., Royer R. A., Fang Y., Yeh G., Fisher A. S., Jeon B. H., and Dempsey B. A. (2002) Theoretical and experimental considerations related to reaction-based modeling: A case study using iron(III) oxide bioreduction. *Geomicrobio. J.* **19**(2), 1–35.
- Caccavo F., Lonergan D. J., Lovley D. R., Davis M., Stolz J. F., and McInerney M. J. (1994) *Geobacter sulfurreducens* sp. nov., a hydrogen- and acetate-oxidizing dissimilatory metal-reducing microorganism. *Appl. Env. Microbio.* **60**, 3752–3759.
- Chen Y. (1994) CIRF: A general coupled reaction-transport model and simulator. Ph.D., Indiana University.
- Chilakapati A. (1995) RAFT. A simulator for reactive flow and transport of groundwater contaminants. PNL-10636. Pacific Northwest National Laboratory. Richland, WA.
- Chilakapati A., Ginn T., and Szecsody J. E. (1998) An analysis of complex reaction networks in groundwater modeling. *Water Res. Res.* **34**, 1767–1780.
- Clark W. M. (1960) Oxidation-Reduction Potentials of Organic Systems. The Williams and Wilkins Co.
- Cummings D. E., Caccavo J. F., Fendorf S. and Rosenzweig R. F. (1999) Arsenic mobilization by the dissimilatory Fe(III)-reducing bacterium *Shewanella alga* BrY. *Env. Sci. Tech.* **33**, 723–729.
- Davis J. A. and Hem J. D. (1989) The Surface Chemistry of Aluminum Oxides and Hydroxides. In *The Environmental Chemistry of Aluminum* (ed. G. Sposito). CRC Press.
- Dzombak D. A. and Morel F. M. M. (1990) Surface Complexation Modeling: Hydrous Ferric Oxide. John Wiley & Sons.
- Fang Y., Yeh G. T. and Burgos W. D. (2003) A General Paradigm to Model Reaction-Based Biogeochemical Processes in Batch Systems. Accepted by *Water Resources Research* November 2002.
- Fein J. B., Daughney C. J., Yee N., and Davis T. A. (1997) A chemical equilibrium model for metal adsorption onto bacterial surfaces. *Geochim. Cosmochim. Acta* **61**, 3319–3328.
- Fendorf S. E. and Li G. (1996) Kinetics of chromate reduction by ferrous iron. *Env. Sci. Tech.* **30**, 1614–1617.
- Fredrickson J. K., Zachara J. M., Kennedy D. W., Dong H., Onstott T. C., Hinman N. W., and Li S.-M. (1998) Biogenic iron mineralization accompanying the dissimilatory reduction of hydrous ferric oxide by a groundwater bacterium. *Geochim. Cosmochim. Acta* **62**(19–20), 3239–3257.
- Fredrickson J. K., Zachara J. M., Kennedy D. W., Duff M. C., Gorby Y. A., Li S. M. W., and Krupka K. M. (2000) Reduction of U(VI) in goethite (alpha-FeOOH) suspensions by a dissimilatory metal-reducing bacterium. *Geochim. Cosmochim. Acta* **64**(18), 3085–3098.
- Fultz M. L. and Durst R. A. (1982) Mediator Compounds for the Electrochemical Study of Biological Redox Systems: A Compilation. *Anal. Chim. Acta* **140**, 1–18.
- Hansel, C. (2002) Personal communication with W. Burgos.
- Jeon B. H., Dempsey B. A., Burgos W. D., and Royer R. A. (2001) Reactions of ferrous iron with hematite. *Coll. Surf. A.* **191**, 41–55.
- Kim S. and Picardal F. W. (1999) Enhanced anaerobic biotransformation of carbon tetrachloride in the presence of reduced iron oxides. *Env. Toxicol. Chem.* **18**, 2142–2150.
- Klausen J., Trober S. P., Haderlein S. B., and Schwarzenbach R. P. (1995) Reduction of substituted nitrobenzenes by Fe(II) in aqueous mineral suspensions. *Env. Sci. Technol.* **29**, 2396–2404.
- Langner H. W. and Inskeep W. P. (2000) Microbial reduction of arsenate in the presence of ferrihydrite. *Env. Sci. Technol.* **34**, 3131–3136.
- Liger E., Charlet L., and Van Cappellen P. (1999) Surface catalysis of uranium(VI) reduction by iron(II). *Geochim. Cosmochim. Acta* **63**(19–20), 2939–2955.
- Lasaga A. C. (1994) Chemical kinetics of water-rock interactions. *J. Geophys. Res.* **99**, 4009–4025.
- Lichtner P. C. and Seth M. S. (1996) User's Manual for MULTIFLO: Part II MULTIFLO 1.0 and GEM 1.0, Multicomponent-multiphase Reactive Transport Model. Southwest Research Institute.
- Liu C., Kota S., Zachara J. M., Fredrickson J. K., and Brinkman C. K. (2001a) Kinetic analysis of the bacterial reduction of goethite. *Env. Sci. Technol.* **35**(12), 2482–2490.
- Liu C., Zachara J. M., Fredrickson J. K., Kennedy D. W., and Dohnalkova A. (2002) Modeling the inhibition of the bacterial reduction of U(VI) by MnO₂(s). *Env. Sci. Technol.* **36**, 1452–1459.
- Liu C., Zachara J. M., Gorby Y. A., Szecsody J. E., and Brown C. F. (2001b) Microbial reduction of Fe(III) and sorption/precipitation on

- Shewanella putrefaciens strain CN32. *Env. Sci. Technol.* **35**, 1385–1393.
- Lovley D. R., Coates J. D., Blunt-Harris E. L., Phillips E. J. P., and Woodward J. C. (1996) Humic substances as electron acceptors for microbial respiration. *Nature* **382**(6590), 445–448.
- Lovley D. R. and Goodwin S. (1988) Hydrogen concentrations as an indicator of the predominant terminal electron-accepting reaction in aquatic sediments. *Geochim. Cosmochim. Acta* **52**, 2993–3003.
- Lovley D. R., Phillips E. J. P., Gorby Y. A., and Landa E. R. (1991) Microbial Reduction of Uranium. *Nature* **350**(6317), 413–416.
- MacQuarrie K. T. B., Sudicky E. A., and Frind E. O. (1990) Simulation of biodegradable organic contaminants in groundwater I. Numerical formulation in principal directions. *Water Res. Res.* **26**, 207–222.
- Newman D. K. and Kolter R. (2000) A role for excreted quinones in extracellular electron transfer. *Nature* **405**, 2396–2404.
- Roden E. E. and Urrutia M. M. (1999) Ferrous iron removal promotes microbial reduction of crystalline iron(III) oxides. *Env. Sci. Technol.* **33**(11), 1847–1853.
- Roden E. E. and Zachara J. M. (1996) Microbial reduction of crystalline iron(III) oxides: Influence of oxide surface area and potential for cell growth. *Env. Sci. Technol.* **30**(5), 1618–1628.
- Royer R. A., Burgos W. D., Fisher A. F., Unz R. F., and Dempsey B. A. (2002) Enhancement of biological reduction of hematite by electron shuttling and Fe(II) complexation. *Env. Sci. Technol.* **36**, 1939–1946.
- Salvage K. M. and Yeh G. T. (1998) Development and application of a numerical model of kinetic and equilibrium microbiological and geochemical reactions (BIOKEMOD). *J. Hydrol.* **20**, 927–952.
- Soetaert K., Herman P. M. J., and Middleburg J. J. (1996) A model of early diagenetic processes from shelf to abyssal depths. *Geochim. Cosmochim. Acta* **60**, 1019–1040.
- Steeffel C. I. and MacQuarrie K. T. B. (1996) Approaches to modeling of reactive transport in porous media. In *Reviews in Mineralogy*, (eds. P. C. Lichtner, C. I. Steefel, and G. H. Oelkers), vol. 34 pp. 84–129. Mineralogical Society of America.
- Steeffel C. I. and van Cappellen P. (1998) Preface: Reactive transport modeling of natural systems. *J. Hydrol.* **209**, 1–7.
- Smith W. R. (1980) *Computational Aspects of Chemical Equilibrium in Complex Systems*. Academic Press, Inc., New York, N. Y.
- Smith, R. W. and Wissen R. W. (1979) *Chemical Engineering Education*, Winter, 1979, p. 26.
- Stone J. J. (2002) The Effect of Zinc on the Biological Reduction of Hematite. Ph.D. dissertation, The Pennsylvania State University, University Park, PA, December, 2002. 104 pages.
- Stumm W. and Morgan J. J. (1996) *Aquatic Chemistry*. John Wiley and Sons.
- Wildung R. E., Gorby Y. A., Krupka K. M., Hess N. J., Li S. W., Plymale A. E., McKinley J. P., and Fredrickson J. K. (2000) Effect of Electron Donor and Solution Chemistry on Products of Dissimilatory Reduction of Technetium by *Shewanella putrefaciens*. *Appl. Env. Microbiol.* **66**(6), 2451–2460.
- Xu T., Pruess K., and Brimhall G. (1999) An improved equilibrium-kinetics speciation algorithm for redox reactions in variably saturated flow systems. *Comp. Geosci.* **25**(6), 655–666.
- Yeh G. T., Burgos W. D., and Zachara J. M. (2001) Modeling and measuring biogeochemical reactions: System consistency, data needs, and rate formulations. *Adv. Env. Res.* **5**, 219–237.
- Yeh G. T., Fang Y. L. and Burgos W. D. (2002) A new paradigm of reaction-based water quality modeling. *Proc. Fifth Intl. Conf. Hydroinform.*
- Yeh G. T. and Tripathi V. S. (1989) A critical evaluation of recent developments in hydrogeochemical transport models of reactive multicomponent systems. *Water Resources Res.* **25**, 93–108.
- Zachara J. M., Fredrickson J. K., Li S.-M., Kennedy D. W., Smith S. C., and Gassman P. L. (1998) Bacterial Reduction of Crystalline Fe₃O₄ Oxides in Single Phase Suspensions and Subsurface Materials. *Am. Mineral.* **83**, 1426–1443.